Pergamon

Control Eng. Practice, Vol. 2, No. 2, pp. 333-340, 1994

0967-0661/94 $6.00 + 0.00

ROBUST TRACKING CONTROL OF TWO-DEGREES-OF-FREEDOM MOBILE ROBOTS

W. Oelen and J. van Amerongen

Department of Electrical Engineering and Mechatronics Research Centre Twente, University of Twente, P.O. Box 217, 7500 AE Enschede, The Netherlands

Abstract. A robust tracking controller for a mobile robot with two degrees of freedom has been developed. It is implemented and tested on a real mobile robot. Where other controllers show decreasing performance for low reference velocities, the performance of this controller depends only on the geometry of the reference trajectory. This allows accurate positioning at low speeds, close to obstacles. The dynamics of the velocity-controlled mobile robot are considered as a perturbed unity transfer from input velocity to actual velocity. It is shown that the tracking controller is robust with respect to these perturbations.

Key Words. Mobile robots, Vehicles, Velocity control, Position control, Robust control, Control engineering

1. INTRODUCTION

A well-known result from non-linear control theory is that it is not possible to stabilize a dynamic system with one or more non-holonomic constraints to a fixed point in state space by means of a smooth static time-invariant state feedback (Brockett, 1983). This can be achieved, however, by means of non-smooth feedback (Canudas de Wit and Sørdalen, 1991; Tilbury *et al.*, 1992) or time varying feedback (Pomet *et al.*, 1992).

Another approach is to develop tracking controllers, which stabilize a non-holonomic system to a non-stationary reference trajectory. This can be achieved, using smooth static time invariant state feedback. The convergence rate of these tracking controllers approaches zero as the velocity of the input reference signal goes to zero, but the tracking controller can be constructed, such that convergence can be written as function of covered distance instead of elapsed time. For a mobile robot (MR) with one non-holonomic constraint, this kind of convergence will be called *geometric convergence*, if for every meter of covered distance the lateral error decreases by a certain factor.

A tracking controller, using smooth static time-invariant state feedback, for a velocity-controlled MR with one non-holonomic constraint has been developed already by Kanayama *et al.* (1990). However, in their analysis they assume the transfer from desired velocity to actual velocity equal to unity. This controller shows geometric convergence for an ideal MR, but in a real-life situation it shows a steady-state error, proportional to the inverse of the reference linear velocity. The steady-state error of the controller, proposed in this paper, is proportional to the inverse of the radius of curvature of the reference trajectory. Hence, its performance does not depend on the reference linear velocity. The effects of the non-ideal behaviour of the MR on the controller performance are investigated and a robustness analysis of the controller is given. Experiments with a real mobile robot have been used to verify the robustness of the tracking controller. This experimental robot system contains two driven wheels and a castor to carry the mechanical structure.

In the next section some preliminary definitions are given. In Section 3 the control structure is explained. In Section 4 an error measure is given, which is suitable and convenient for describing the deviation from the reference trajectory. A state space model is derived in Section 5, where the error measure of Section 4 serves as the vector of state variables and in Section 6 a feedback law is derived, which stabilizes the model of Section 5. Section 7 contains some simulation results. In Section 8 the practical setup, used for experiments is described and in Section 9 experimental results are given. Finally some conclusions are given in Section 10.

2. PRELIMINARY DEFINITIONS

An ideal MR with two degrees of freedom can be regarded as a system with two inputs: *linear*

velocity (v) and *angular velocity* (ω), both relative to the world. The *pose* (position and orientation) of an MR can be described by using three coordinates $(x\ \ y\ \ \varphi)^T$. The variables x, y and φ are the three state variables of the ideal MR with two degrees of freedom. For the representation of the pose the symbol $\boldsymbol{p}$ is used. For $(v\ \omega)^T$ the symbol $\boldsymbol{v}$ is used. The vector $\boldsymbol{p}$ depends on the coordinate system, which is used to describe positions in the fixed world; the vector $\boldsymbol{v}$ is not affected by a particular choice of the fixed-world coordinate system.

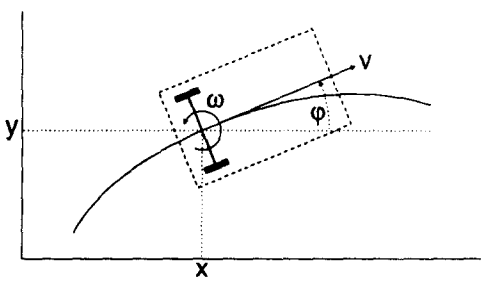

Fig. 1. Pose, linear velocity, and angular velocity

Throughout this paper the reference pose and reference linear and angular velocity are denoted by $\boldsymbol{p}_{ref} = (x_{ref}\ \ y_{ref}\ \ \varphi_{ref})^T$ and $\boldsymbol{v}_{ref} = (v_{ref}\ \ \omega_{ref})^T$. Steady-state values of signals are denoted by a subscript $_{ss}$.

3. THE CONTROLLER STRUCTURE

A real MR with two degrees of freedom can be described in two stages. The first stage contains the dynamics, with two control inputs I_1 and I_2 (e.g. motor currents) and two outputs v and ω. The second stage contains the kinematics (transfer from $\boldsymbol{v}$ to $\boldsymbol{p}$). An ideal MR can be described completely by the kinematics. The kinematics are given below:

$$\dot{x} = v\cos(\varphi) \tag{1a}$$

$$\dot{y} = v\sin(\varphi) \tag{1b}$$

$$\dot{\varphi} = \omega. \tag{1c}$$

It is assumed that v, ω, x, y and φ can all be measured or estimated with reasonable accuracy.

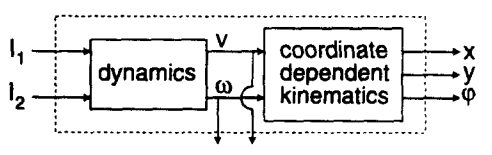

Fig. 2. Two-stage model of real MR

The controller structure for a real MR can also be decomposed in two stages. An inner loop (see Fig. 3), depending on the MR dynamics, can be used for controlling the linear and angular velocity of the MR. An outer loop (see Fig. 4) controls the pose of the MR. This paper focuses on the outer-loop pose controller.

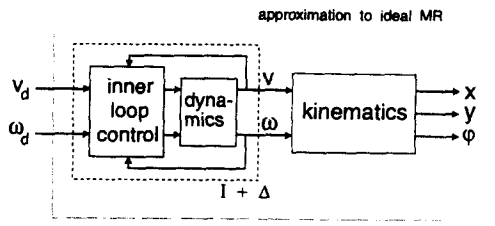

Fig. 3. Model of MR with non-ideal inner loop I+Δ

Ideally the behaviour of the velocity-controlled MR is given by equations (1a,b,c), with $v=v_d$ and $\omega=\omega_d$, where v_d and ω_d are the input signals for the velocity-controlled MR (see Figs 3 and 4). In a real-life situation there will be a difference between v and v_d and ω and ω_d, due to incompletely compensated dynamics of the MR. A non-ideal velocity-controlled MR is represented by a block with transfer I+Δ (see Figs 3 and 4), where I is the unity transfer and Δ is a perturbation. In general the structure of Δ is unknown. The only assumption on Δ is that it is possible to determine an upper bound for it (see App. A).

In the outer loop the difference between $\boldsymbol{p}_{ref}$ and $\boldsymbol{p}$ is translated into a correction δv_{ref}, which is added to v_{ref}, and a correction $\delta\omega_{ref}$, which is added to ω_{ref}.

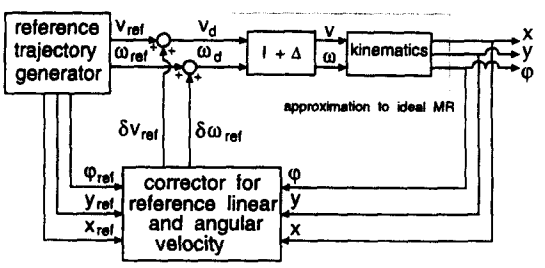

Fig. 4. Structure of outer-loop pose controller

4. A MEASURE OF THE POSE ERROR

The error of the pose can be represented by

$$\Delta\boldsymbol{p} = (\Delta x\ \Delta y\ \Delta\varphi)^T = \boldsymbol{p}\text{-}\boldsymbol{p}_{ref}. \tag{2}$$

This vector depends on the orientation of the MR. It can be made orientation-independent by using a coordinate system, which is fixed relative to the MR. This new representation is written as

$$\Delta\boldsymbol{p}^v = (\Delta x^v\ \Delta y^v\ \Delta\varphi^v)^T \tag{3}$$

where the superscript ^{v} denotes the change of the coordinate system. Here Δx^v is the error in driving direction, Δy^v is the lateral error and $\Delta\varphi^v$ is the orientation error (see Fig. 5).

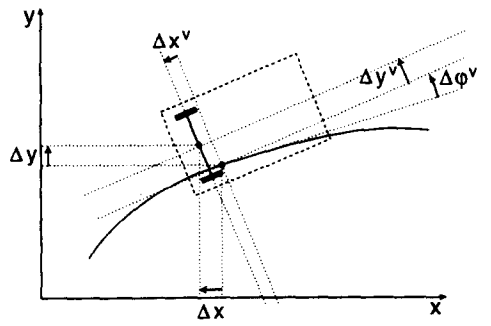

Fig. 5. Pose error, in world-fixed and MR-fixed frame

The pose error as it is defined here is specified by three quantities. Using the properties of an MR with one non-holonomic constraint the number of error quantities can be reduced by one.

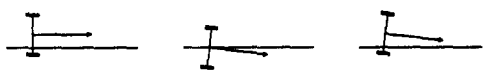

Fig. 6. Three error situations

In Fig. 6 three possible situations are given, of which the third situation is the best if one wants to steer the MR towards the reference trajectory. The orientation error should not be steered to zero, while the lateral error is non-zero. It is better to have an orientation error which is proportional to the lateral error. Hence the controller objective should be to steer $\Delta\varphi^v$ to $-\alpha\Delta y^v \text{sign}(v_{ref})$, where α is a positive constant and where the factor $\text{sign}(v_{ref})$ takes into account the desired direction of motion. Now a measure $\Delta z^v=\Delta\varphi^v+\alpha\Delta y^v \text{sign}(v_{ref})$ for the orientation error can be introduced, which replaces $\Delta\varphi^v$. This results in a new pose error $\Delta\boldsymbol{p}^{v'}$:

$$\Delta\boldsymbol{p}^{v'} = (\Delta x^v \;\; \Delta y^v \;\; \Delta z^v)^T. \tag{3'}$$

Because of the non-holonomic constraint of the MR it is not possible to compensate Δy^v directly. In App. B it is shown that if Δz^v equals zero, then Δy^v shows geometric convergence. Hence the error can be specified by the two quantities Δx^v and Δz^v only.

5. THE ERROR DYNAMICS

In Section 5.1 the error dynamics are derived, as a function of the difference between actual velocity and reference velocity. In Section 5.2 the difference between actual velocity and reference velocity is split into a user-controllable part and a perturbation part. From this a state-space model is derived, with two control inputs and two perturbations.

5.1. *The pose error*

A state-space model of the dynamics of the pose error can be derived from equations (1a,b,c) and (2). The time derivative of $\Delta\boldsymbol{p}$ can be written as

$$\Delta\dot{\boldsymbol{p}} = \begin{pmatrix} c\varphi\, v - c\varphi_{ref}\, v_{ref} \\ s\varphi\, v - s\varphi_{ref}\, v_{ref} \\ \omega - \omega_{ref} \end{pmatrix}. \tag{4}$$

Here $c\varphi$ stands for $\cos(\varphi)$ and $s\varphi$ stands for $\sin(\varphi)$. A similar notation is used for $\cos(\varphi_{ref})$ and $\sin(\varphi_{ref})$. By writing φ_{ref} as $\varphi-\Delta\varphi$, equation (4) can be rewritten as a product of a rotation matrix (coordinate transformation) and a vector represented in coordinates of a base, fixed to the MR.

$$\Delta\dot{\boldsymbol{p}} = \begin{pmatrix} c\varphi & -s\varphi & 0 \\ s\varphi & c\varphi & 0 \\ 0 & 0 & 1 \end{pmatrix} \begin{pmatrix} v - \cos(\Delta\varphi)\, v_{ref} \\ \sin(\Delta\varphi)\, v_{ref} \\ \omega - \omega_{ref} \end{pmatrix} \tag{5}$$

In order to find an expression for $\Delta\dot{\boldsymbol{p}}^v$ consider the relation between $\Delta\boldsymbol{p}$ and $\Delta\boldsymbol{p}^v$, given by

$$\Delta\boldsymbol{p}^v = \begin{pmatrix} c\varphi & s\varphi & 0 \\ -s\varphi & c\varphi & 0 \\ 0 & 0 & 1 \end{pmatrix} \Delta\boldsymbol{p}. \tag{6}$$

Differentiation of this relation yields the following:

$$\Delta\dot{\boldsymbol{p}}^v = \begin{pmatrix} c\varphi & s\varphi & 0 \\ -s\varphi & c\varphi & 0 \\ 0 & 0 & 1 \end{pmatrix} \Delta\dot{\boldsymbol{p}} + \omega \begin{pmatrix} -s\varphi & c\varphi & 0 \\ -c\varphi & -s\varphi & 0 \\ 0 & 0 & 0 \end{pmatrix} \Delta\boldsymbol{p}. \tag{7}$$

Using equation (5) and the inverse of equation (6), one finds an expression for $\Delta\dot{\boldsymbol{p}}^v$, which does not depend on the orientation of the MR.

$$\Delta\dot{x}^v = v - \cos(\Delta\varphi^v)\, v_{ref} + \omega\Delta y^v \tag{8a}$$
$$\Delta\dot{y}^v = \sin(\Delta\varphi^v)\, v_{ref} - \omega\Delta x^v \tag{8b}$$
$$\Delta\dot{\varphi}^v = \omega - \omega_{ref} \tag{8c}$$

Replacing v by $v_{ref}+\Delta v$ and ω-ω_{ref} by $\Delta\omega$ yields equations in a form which is more suitable for the analysis, given in the next sub-section.

$$\Delta\dot{x}^v = \Delta v + (1-\cos(\Delta\varphi^v))\, v_{ref} + \omega\Delta y^v \tag{9a}$$
$$\Delta\dot{y}^v = \sin(\Delta\varphi^v)\, v_{ref} - \omega\Delta x^v \tag{9b}$$
$$\Delta\dot{\varphi}^v = \Delta\omega \tag{9c}$$

5.2. *The input signals and perturbations*

The signal Δv can be written as the sum of an input signal δv_{ref} and a perturbation ξ_v. Similarly $\Delta\omega$ can be written as $\delta\omega_{ref}+\xi_\omega$ (see Fig. 4). Using this structure the model of equations (9a,b,c) can be written as a state space model with input signals δv_{ref} and $\delta\omega_{ref}$ and perturbation signals ξ_v and ξ_ω.

$$\Delta\dot{x}^v = \delta v_{ref} + (1-\cos(\Delta\varphi^v))\, v_{ref} + \omega\Delta y^v + \xi_v \tag{10a}$$
$$\Delta\dot{y}^v = \sin(\Delta\varphi^v)\, v_{ref} - \omega\Delta x^v \tag{10b}$$
$$\Delta\dot{\varphi}^v = \delta\omega_{ref} + \xi_\omega \tag{10c}$$

6. A STABILIZING CONTROLLER

The error dynamics of the closed-loop system can be described by means of only two state variables Δx^v and Δz^v. This can be reached by rearranging the state space model (10a,b,c) and using a linearizing and stabilizing state feedback for Δx^v and Δz^v. Furthermore a steady-state robustness analysis is given of the resulting closed-loop system.

6.1. *Reduction of number of states in closed loop*

The controller shown in this section stabilizes Δx^v and Δz^v. A model for these two states can be derived from (10a,b,c):

$$\Delta \dot{x}^v = \delta v_{ref} + (1-\cos(\Delta\varphi^v))v_{ref} + \omega\Delta y^v + \xi_v \quad (11a)$$

$$\Delta \dot{z}^v = \delta\omega_{ref} + \alpha\sin(\Delta\varphi^v)|v_{ref}| - \alpha\omega\Delta x^v \mathrm{sign}(v_{ref}) + \xi_\omega \quad (11b)$$

By means of the stabilizing feedback, given in (12a,b), the explicit reference to Δy^v and $\Delta\varphi^v$ is removed. The result is a system with two state variables Δx^v and Δz^v only. This is given in (13a,b).

$$\delta v_{ref} = -K_x\Delta x^v - (1-\cos(\Delta\varphi^v))v_{ref} - \omega\Delta y^v \quad (12a)$$

$$\delta\omega_{ref} = -K_z\Delta z^v - \alpha\cdot\sin(\Delta\varphi^v)|v_{ref}| + \alpha\omega\Delta x^v \mathrm{sign}(v_{ref}) \quad (12b)$$

$$\Delta \dot{x}^v = -K_x\Delta x^v + \xi_v \quad (13a)$$

$$\Delta \dot{z}^v = -K_z\Delta z^v + \xi_\omega \quad (13b)$$

Here K_x and K_z are positive constants.

The first-order system with feedback (13a,b) has good robustness properties (see App. A). In App. B it is shown that convergence of Δx^v and Δz^v implies geometric convergence of Δy^v and $\Delta\varphi^v$.

6.2. *Steady state errors of closed-loop system*

For steady states the time derivatives of Δx^v, Δy^v, Δz^v and $\Delta\varphi^v$ can be assumed equal to zero. $\Delta x^v{}_{ss}$ and $\Delta z^v{}_{ss}$ are equal to $\xi_{v,ss}/K_x$ and $\xi_{\omega,ss}/K_z$. Equations (8c) and (10c) reduce to $\omega_{ss}=\omega_{ref}$ and $\delta\omega_{ref,ss}=-\xi_{\omega,ss}$. Substituting these values in equation (12b) the following steady-state equation for Δy^v and $\Delta\varphi^v$ can be derived.

$$\sin(\Delta\varphi^v{}_{ss})v_{ref} = \omega_{ref}\Delta x^v{}_{ss} \quad (14)$$

If ω_{ref}/v_{ref} becomes too large in magnitude then there will be no $\Delta\varphi^v{}_{ss}$, which satisfies (14). In that case no steady state exists (simulations show that for increasing ω_{ref}/v_{ref} the steady state bifurcates into a limit cycle). This problem can simply be overcome by imposing a lower bound on the radius of curvature of the reference trajectory. In the tracking controller developed by Kanayama *et al.* (1990), a problem arises if $\xi_{\omega,ss}/v_{ref}$ becomes large in magnitude (see App. C). This situation is worse, because in general it cannot be guaranteed that $\xi_{\omega,ss}$ is small.

The steady-state error of Δx^v can be removed by adding an integrating term $-K_i\int\Delta x^v dt$ to the feedback of δv_{ref}, but the price to be paid is a reduction in stability robustness.

6.3. *The controller parameters*

The controller developed here has three parameters (α, K_x and K_z). If the integrating feedback is used then a fourth parameter K_i is introduced.

The larger the constant α, the more strongly the controller steers the MR towards the reference trajectory. It should be chosen, such that the order of magnitude of $\alpha\Delta y^v$ is close to the order of magnitude of $\Delta\varphi^v$, during normal operation. For a system operating at lateral errors, in the order of magnitude of 10 cm, a value of α=1 works fine.

Larger K_x and K_z reduce the steady-state error and make convergence faster. However, their values are limited by the state-dependent perturbations ξ_v and ξ_ω (see app. A). Another limitation is that the time constants $1/K_x$ and $1/K_z$ should be larger than the sampling time of the robot system.

If integrating feedback is used then the error Δx^v shows approximate second-order behaviour with relative damping equal to $\frac{1}{2}K_x/\sqrt{K_i}$. For fastest response without overshoot (critical damping) it is best to choose K_i equal to $\frac{1}{4}K_x^2$.

7. SIMULATION RESULTS

For the simulations a model of I+Δ (i.e. a velocity-controlled MR) is used, with a linear velocity deadband d_v, and angular velocity deadband d_ω. If $|v_d|>d_v$, then the velocity deadband introduces a velocity perturbation $\xi_v=d_v\,\mathrm{sign}(v_d)$, else $\xi_v=v_d$. The angular velocity perturbation ξ_ω has a similar form.

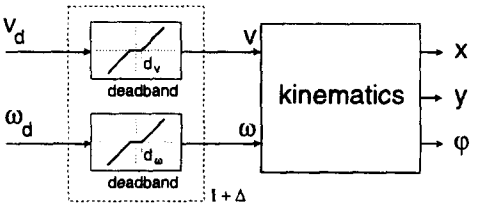

Fig. 7. Model used for simulation

The reference trajectory used for the simulations is a circle with radius v_{end}/ω_{end}, where v_{end} and ω_{end} are the final reference velocities (see Fig. 8). For $0\le t\le 2$ the reference velocities are equal to zero. Between t=2 and t=4 they go to their final values smoothly. If ω_{end} equals zero then the circle reduces to a line.

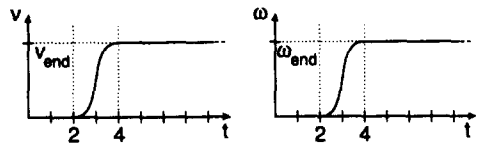

Fig. 8. Reference velocity signals

Four sets of simulation results are shown.

1) Ideal MR: $d_v=0$, $d_\omega=0$
   Controller parameters: $K_x=K_z=5$; $\alpha=1$; $K_i=0$
   Ref. signals: v_{end}, see fig. 9; $\omega_{end}=0$
   Initial errors: $\Delta x^v=0.04$; $\Delta y^v=-0.08$; $\Delta\varphi^v=-0.02$
2) As 1, but now $d_v=0.05$
3) $d_v=0.07$, $d_\omega=0.05$
   Controller parameters: $K_x=K_z=2$; $\alpha=1$; $K_i=0$
   Ref. signals: v_{end}, see fig. 11; $\omega_{end}=1$
   Initial errors: $\Delta x^v=0$; $\Delta y^v=0$; $\Delta\varphi^v=0$
4) As 3, but now $\omega_{end}=v_{end}$, instead of $\omega_{end}=1$.

Each figure below contains the result of a set of three or four simulations. In each simulation the errors Δx^v and Δy^v (in meters), and Δz^v (in radians), are plotted as function of time in seconds. In each figure this is done for different reference signals.

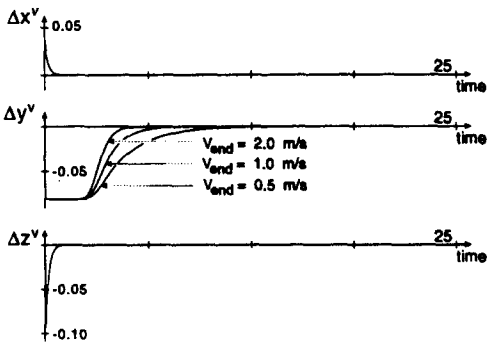

Fig. 9. Simulations 1, along straight line, ideal MR

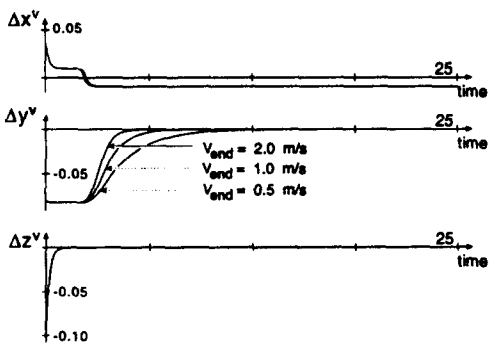

Fig. 10. Simulations 2, along straight line, deadband

The simulations show that compensation of Δx^v and Δz^v starts immediately, but compensation of the lateral error Δy^v only starts once the MR starts moving. For motion along a straight line, a velocity deadband introduces a steady-state error in driving direction, but no lateral and orientation error are introduced. The simulations also show that for lower v_{ref} the convergence of the lateral error Δy^v becomes slower, but in terms of covered distance the convergence is the same for all v_{ref}. The lateral error converges to zero geometrically.

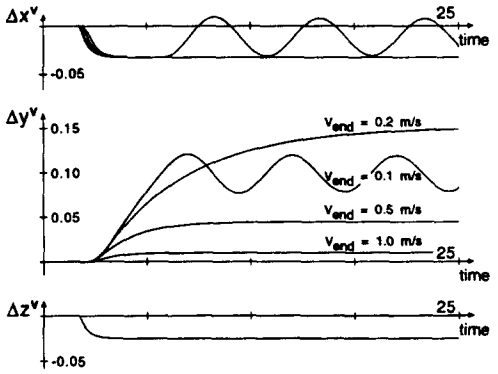

Fig 11. Simulations 3, constant angular velocity

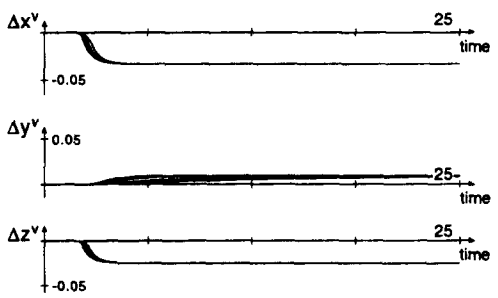

Fig. 12. Simulations 4, constant radius of curvature

Fig. 11 shows that for decreasing radius of curvature v_{end}/ω_{end} the steady-state error increases, until a situation is reached where there does not exist a steady state anymore. Figure 12 shows that for constant radius of curvature the controller behaves well for all four reference velocities used.

8. MOBILE AUTONOMOUS ROBOT TWENTE

The controller as it is proposed here has been tested on the MART-robot, where MART is an acronym for Mobile Autonomous Robot Twente. This MR was developed at the Mechatronics Research Centre Twente. The goal of the MART-project is to gain insight in how to design complex mechatronic systems. This insight should be demonstrated by the design and realization of an automated assembly system. This project results from a preliminary study by Abrahams (1985), who developed a concept for a future automated assembly hall. Instead of assembly of products on a conveyor belt, Abrahams proposed a more flexible and more robust system, where a set of mobile robots takes care of the assembly tasks. In Abrahams' concept, each mobile robot consists of a vehicle, which carries a manipulator. Assembly can be done on the vehicle (also during motion for increased

throughput) and on fixed work stations. The concept of Abrahams allows the use of 2 DOF mobile robots, as long as they can be positioned sufficiently accurately.

8.1 *The mechanical structure of the mobile robot*

The vehicle is split in two parts, where both parts are connected to each other by means of soft springs. The lower part contains the wheels and the motors for driving the wheels. The upper part of the vehicle carries the manipulator and the batteries and contains the necessary electronics. The soft springs provide a good suspension, without the need of very soft tyres. In Fig. 13 a schematic drawing of the mobile robot is given.

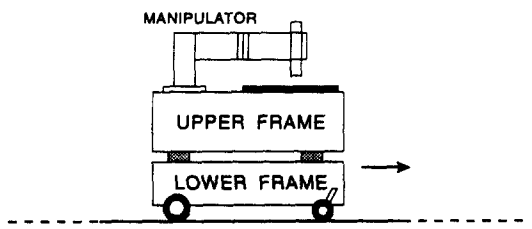

Fig. 13. Schematic drawing of the MART-robot

The lower part of the vehicle has a mass of 75 kg and the upper part of the vehicle has a mass of 400 kg. The dominant resonance frequency of the suspended upper frame is 3 Hz in all directions. The length of the vehicle is 1.4 meter, its width is 1.0 meter and its height is 0.8 meter. The vehicle has two driven wheels and one castor. The castor limits the steering capabilities, because of coulomb friction. This is especially true when the castor flips from forward to backward orientation or vice versa.

8.2. *The velocity controller*

The tracking controller is designed for an MR with velocity inputs. The MART-robot, however, has two input currents. This problem is overcome by applying velocity control to the mobile robot. This velocity control is the inner-loop control, mentioned in Section 3. A simple planar dynamical model is used for compensation of coulomb friction in the motors and rolling friction in the driven wheels. Centripetal forces are compensated as well. Friction in the castor is not compensated. A linear feedback law is superimposed on the compensation. Figs 14 and 15 illustrate the performance of the velocity controlled MART-robot. Both the reference signals (dashed lines) and the measured actual signals are given in the same figures.

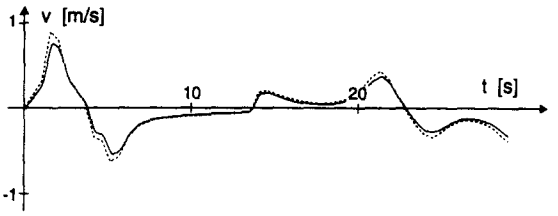

Fig. 14. Reference and measured v

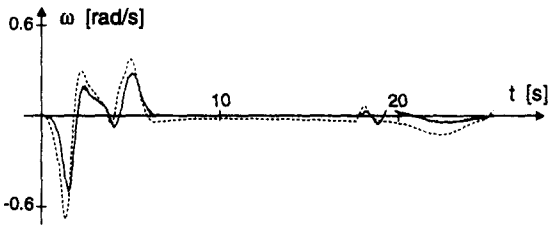

Fig. 15. Reference and measured ω

Figs 14 and 15 show that the performance of the velocity-controlled MR is only moderate, hence the perturbation Δ is fairly large. Especially the magnitude of the angular velocity tracking error is quite large. This is due to uncompensated friction in the castor.

8.3. *Practical setup of the control system*

The tracking controller is implemented in OCCAM on a T800 transputer, running at 25 MHz. On the same transputer the velocity controller and some I/O processes (file I/O, screen output and AD/DA conversion) are running. The vehicle is connected to an 80386 host PC, by means of a 10 Mbit/s transputer link. The controllers run at a sampling rate of 100 Hz. This is well above the main resonance frequencies of the mechanical structure, which are at 3 Hz and 20 Hz.
In the present situation measuring the position and orientation of the vehicle is done by integrating wheel revolutions (odometry).

9. EXPERIMENTAL RESULTS

Two types of experiments have been done with the MART-robot. In one set of experiments the MR has to follow a straight line, 4 meters in length. In these experiments there is an initial lateral error of 10 cm. In the other set of experiments more-complex reference trajectories are used. There is no initial error in the second set of experiments.
In all experiments the constant α was chosen equal to 1. The constants K_x and K_z were chosen equal to 10. The time constants $1/K_x$ and $1/K_z$ are well above the sampling time of the controller and they do not interfere strongly with the resonance frequencies in the mechanical structure of the mobile robot. No integrating feedback is used in the experiments.

In the first set of experiments a final accuracy of better than 1 cm could be achieved for any reference velocity varying smoothly in the range from 0 m s^{-1} to 0.6 m s^{-1}. More interesting, however, is the behavior of the MR if it has to move along a trajectory with varying radius of curvature.

A typical trajectory used in the second set of experiments is given in Fig. 16.

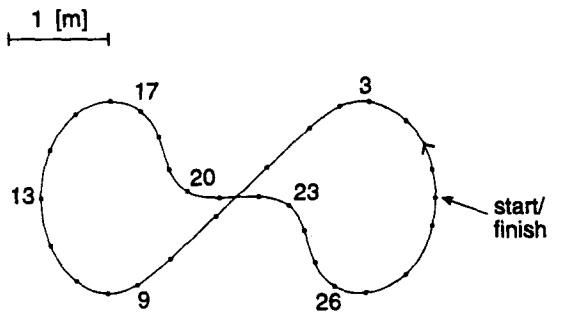

Fig. 16. Reference trajectory for MART-robot

The total time taken for the trajectory is 30 seconds; the total length of the trajectory is approximately 12 meters. One-second intervals are marked on the trajectory by means of dots. After 13 seconds the maximum distance (4 meters) from the start is reached. After another 17 seconds the MR reaches the finish, which is at the same place as the start. The velocity profile along the trajectory is smooth. The MR starts with zero velocity and finishes with zero velocity. During motion along this trajectory the pose error $\Delta \boldsymbol{p}^v$ is monitored. In order to present the results in a more compact way the absolute error $\Delta r^v = \|(\Delta x^v \ \Delta y^v)^T\|$ is given, instead of the individual quantities Δx^v and Δy^v. Here $\|\cdot\|$ denotes the standard Euclidian norm of a vector in $\mathbf{R}^2$. The results are given below.

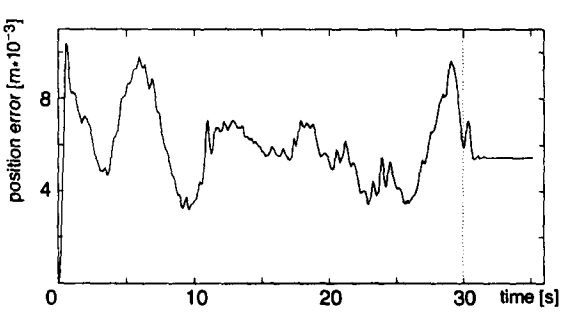

Fig. 17. The absolute error as function of time

Fig. 17 shows that during almost the entire trajectory the absolute error remains below 1 cm. The experiments with the MART-robot show that the tracking controller performs well, also on more complex reference trajectories. It should be kept in mind that the underlying velocity-controlled MR has only moderate performance (see Figs 14 and 15).

10. CONCLUSIONS

In this paper a pose controller is proposed, whose performance depends only on the shape of the reference trajectory. It is shown that the controller is robust with respect to perturbations. These properties could be achieved by introducing a new error measure, which relates the desired orientation of the mobile robot to the actual lateral error.

The pose controller is simulated on a non-ideal MR. A deadband perturbation is used to simulate static velocity tracking errors, which may occur in a real velocity-controlled MR. These simulations confirm the robustness of the pose controller with respect to perturbations.

Experimental results on a mobile robot, developed at the Mechatronics Research Centre Twente, show that the tracking controller performs well, even if the underlying velocity-controlled MR only performs moderately.

The controller is computationally very simple. Only the simple feedback laws (12a,b) and the pose error in MR-fixed coordinates (6) have to be computed in real time.

11. REFERENCES

Abrahams J. (1985). Zeer voorlopig onderzoek naar flexibele assemblage systemen (in Dutch). *Internal Report CFT*, Philips Eindhoven. The Netherlands

Brockett, R.W. (1983). Asymptotic stability and feedback stabilization. In: *Differential Geometric Control Theory*, (R.W. Brockett, R.S. Millman, and H.J. Sussman, Eds.), pp. 181-191. Birkhäuser.

Canudas de Wit, C., and O.J. Sørdalen (1991). Exponential Stabilization of Mobile Robots with Nonholonomic Constraints. *IEEE Conference on Decision and Control*, 692-697.

Kanayama, Y., Y. Kimura, F. Miyazaki and T. Noguchi (1990). A stable tracking control method for an autonomous mobile robot. *Proc. IEEE 1990 International Conference on Robotics and Automation.*, **1**, 384-389

Pomet J.-B., B. Thuilot, G. Bastin, and G. Campion (1992). A hybrid strategy for the feedback stabilization of nonholonomic mobile robots. *Proc. IEEE 1992 International Conference on Robotics and Automation.*, **1**, 129-134

Tilbury, D., J.-P. Laumond, R. Murray, S. Sastry, and G. Walsh (1992). Steering Car-Like Systems with Trailers Using Sinusoids. *Proc. IEEE 1992 International Conference on Robotics and Automation.*, **3**, 1993-1998

APPENDIX A

In this appendix the effect of the linear velocity tracking error ξ_v of the velocity-controlled MR on the stability of the pose controller is investigated (see Figs 3 and 4). Assume that positive constants A_1, A_2 and A_3 exist, such that for all v_d and $\dot{v}_d$

$$|\xi_v| < A_1 + A_2|v_d| + A_3|\dot{v}_d|. \tag{15}$$

This assumption is a reasonable one. In general, a controller should have a certain error bound in order to be useful. Here the analysis is simplified by considering straight-line motion only ($\omega=0$ and $\varphi=0$). In that case v_d can be written as $v_{ref}-K_x\Delta x^v$. Now the following can be derived for (13a):

$$\Delta\dot{x}^v = -K_x\Delta x^v \pm A_1 \pm A_2(v_{ref}-K_x\Delta x^v) \pm A_3(\dot{v}_{ref}-K_x\Delta\dot{x}^v). \tag{16}$$

From (16) a worst-case equation can be derived (choosing the worst-case signs of the ±'s):

$$\Delta\dot{x}^v = -K_x\frac{1-A_2}{1-A_3K_x}\Delta x^v + \frac{A_1+A_2v_{ref}+A_3\dot{v}_{ref}}{1-A_3K_x}. \tag{17}$$

Eq. (17) shows that stability is guaranteed, if both $A_2<1$ and $A_3K_x<1$. For a useful velocity controller, the first constraint is generally satisfied. The second constraint requires that K_x is not chosen too large.

The analysis given here only gives an impression of the robustness of the controller. A more complete, but similar analysis can be given for general motion (taking into account both ξ_v and ξ_ω), but the computational details are more involved.

APPENDIX B

Suppose Δx^v and Δz^v converge to zero. Once Δx^v and Δz^v are small the following equation can be derived from $\Delta z^v=\Delta\varphi^v+\alpha\Delta y^v\,\mathrm{sign}(v_{ref})$ and (10b):

$$\Delta\dot{y}^v = -\sin(\alpha\Delta y^v)|v_{ref}|. \tag{18}$$

Now suppose $0\le\Delta y^v\le\frac{1}{2}\pi/\alpha$ (hence $0\le\Delta\varphi^v\le\frac{1}{2}\pi$). This is a very weak constraint on the initial error. In that case $\sin(\alpha\Delta y^v)\ge 2\alpha\Delta y^v/\pi$. The convergence rate of Δy^v is at least as large as the convergence rate of γ from the system below.

$$\dot{\gamma} = -2\alpha\gamma|v_{ref}|/\pi \tag{19}$$

The variable γ converges to zero with a time constant $\frac{1}{2}\pi/(\alpha|v_{ref}|)$. The time constant becomes infinitely large if v_{ref} approaches 0. It is better to describe convergence as function of covered distance, which can be written as $l=\int|v_{ref}|dt$. Differentiation yields $dl=|v_{ref}|dt$. Using this, (19) can be rewritten as

$$d\gamma = -\frac{2}{\pi}\alpha\gamma|v_{ref}|\,dt = -\frac{2}{\pi}\alpha\gamma\,dl. \tag{20}$$

Now the dynamical behaviour of γ can be described in terms of covered distance. It converges to 0 geometrically, with a 'distance constant' $\frac{1}{2}\pi/\alpha$.

APPENDIX C

Kanayama *et al.* use the following feedback:

$$\delta v_{ref} = -K_x\Delta x^v - (1-\cos(\Delta\varphi^v))v_{ref} \tag{21a}$$
$$\delta\omega_{ref} = -(K_y\Delta y^v + K_\varphi\sin(\Delta\varphi^v))v_{ref} \tag{21b}$$

Using this feedback and equations (10a,b,c), the system with feedback can be derived easily.

$$\Delta\dot{x}^v = -K_x\Delta x^v + \omega\Delta y^v + \xi_v \tag{22a}$$
$$\Delta\dot{y}^v = \sin(\Delta\varphi^v)v_{ref} - \omega\Delta x^v \tag{22b}$$
$$\Delta\dot{\varphi}^v = -(K_y\Delta y^v + K_\varphi\sin(\Delta\varphi^v))v_{ref} + \xi_\omega \tag{22c}$$

This system converges to a zero equilibrium state for perturbations equal to zero and $v_{ref}>0$ (Kanayama *et al.*, 1990). For steady-state and non-zero perturbations, (22c) becomes as follows:

$$(K_y\Delta y^v{}_{ss} + K_\varphi\sin(\Delta\varphi^v{}_{ss}))v_{ref} = \xi_{\omega,ss} \tag{23}$$

Eq. (23) shows that a problem arises if $\xi_{\omega,ss}/v_{ref}$ becomes large. In the controller proposed in this paper a problem arises if ω_{ref}/v_{ref} becomes large.